buildings

MDPI

Article

An Investigation of the Behaviors and Characteristics of the Interfacial Bonding Capacity between Cement Emulsified Asphalt Composite Binder and Reclaimed Asphalt Pavement

Kangfeng Zheng [1], Qing Yang [1,*], Xin Qiu [1], Wenyi Xu [2,*], Huiqiong Liu [3] and Zijun Chen [1]

[1] Road and Traffic Engineering Institute, College of Engineering, Zhejiang Normal University, Jinhua 321004, China; kangfeng@zjnu.edu.cn (K.Z.); xqiu@zjnu.cn (X.Q.); czijun@zjnu.edu.cn (Z.C.)
[2] Key Laboratory of Road and Traffic Engineering of the Ministry of Education, Tongji University, Shanghai 200092, China
[3] State Key Laboratory of Rail Transit Vehicle System, Southwest Jiaotong University, Chengdu 610031, China; hqliu@my.swjtu.edu.cn
* Correspondence: yangq@zjnu.cn (Q.Y.); wenyixu@tongji.edu.cn (W.X.)

Abstract: The interfacial bonding capacity between cement emulsified asphalt composite binder (CEACB) and reclaimed asphalt pavement (RAP) plays a critical role in improving the pavement performance of cold recycled asphalt emulsion mixtures (CRAEMs). This study aims to investigate the formation and development of the interfacial bonding capacity between CEACB and RAP. First, the dynamic wettability and the spreading behaviors of CEACB on RAP surfaces were explored according to the surface free energy theory. Second, digital image processing (DIP) technology was employed to recognize interfacial failure patterns. Lastly, the influence of internal and external factors on the interfacial bonding capacity between CEACB and RAP during the curing process was analyzed via grey relational analysis (GRA). The results indicate that a moderate cement content with a mass ratio of asphalt to cement equivalent to 1.0 can significantly enhance the wettability of CEACB on RAP surfaces. By appropriately prolonging the curing time and controlling the curing temperature, it is possible to increase the bonding strength between CEACB and RAP. Additionally, a strong correlation exists between initial wettability and ultimate bonding capacity during the bonding strength curing process. The good wettability that developed in the initial stage of interfacial strength formation relates to the decreased spalling rate of CEACB on the RAP surface. This study is not only devoted to understanding the mechanisms that can enhance CRAEM performance but also provides important guidance for practical engineering applications of cold recycled asphalt pavements.

Keywords: cement emulsified asphalt composite binder; initial wettability; bonding strength; contact angle; surface free energy; grey relational analysis

Citation: Zheng, K.; Yang, Q.; Qiu, X.; Xu, W.; Liu, H.; Chen, Z. An Investigation of the Behaviors and Characteristics of the Interfacial Bonding Capacity between Cement Emulsified Asphalt Composite Binder and Reclaimed Asphalt Pavement. *Buildings* **2024**, *14*, 1217. https://doi.org/10.3390/buildings14051217

Academic Editor: Flávio De Andrade Silva

Received: 14 March 2024
Revised: 7 April 2024
Accepted: 20 April 2024
Published: 25 April 2024

1. Introduction

In response to the sustainable development goals emphasizing energy conservation and emission reduction, cold recycling technology for asphalt pavement has emerged as a focus in the field of pavement engineering [1,2]. Specifically, emulsified asphalt cold recycling technology has attracted extensive attention due to numerous environmental advantages such as low-temperature construction, low carbon dioxide emissions, and its high utilization of reclaimed asphalt pavement (RAP) [3–6]. Nevertheless, the existence of aged asphalt films on RAP surfaces affects the demulsification rate of emulsified asphalt, leading to insufficient initial bonding strength between RAP and emulsified asphalt, which impedes the developmental processes relating to the strength of cold recycled asphalt emulsion mixtures (CRAEMs) [7]. Actually, cement emulsified asphalt composite binder (CEACB) added to cement with additives would effectively and significantly enhance the initial strength of CRAEM compared with the use of emulsified asphalt binder alone [8].

Oruc et al. [9] applied a series of laboratory tests to evaluate material characteristics such as creep, water damage, strength, etc., and demonstrated that the addition of cement could significantly improve the mechanical properties of emulsified asphalt mixtures. Rutherford et al. [10] conducted an extensive investigation on the mechanical properties of CEACB through the use of compressive tests, relaxation tests, and microstructural analysis, which indicated that CEACB, with the characteristic rigidity of cement and flexibility of asphalt, could exert a substantial impact on the pavement performance of CRAEMs. Therefore, it is believed that the strength development of CRAEMs not only depends on the properties of the key component—CEACB—but is also closely related to the interface bonding properties between CEACB and RAP.

Generally, the interface between CEACB and RAP pertains to a minuscule yet potentially vulnerable area in CRAEMs, which is directly related to the strength formation and development of CRAEMs [11]. Currently, various theories are employed to explain the interfacial bonding mechanisms between CEACB and RAP, including weak boundary theory [12], chemical reaction theory [13], mechanical theory [14], surface energy theory [15], and electrostatic theory [16]. It is noteworthy that surface energy theory has gained prominence in explaining the interfacial bonding capacity between asphalt binders and aggregates. According to surface energy theory, good wettability means that a CEACB could coat a larger area of RAP more quickly, thereby enhancing the ultimate bonding capability [17,18]. Researchers have made significant progress in identifying the influencing factors of wettability and evaluation methods [19]. For instance, Fang et al. [20] employed surface energy theory to investigate the wetting behavior at the interface between rejuvenators and aged asphalt, which indicated that elevated temperatures and prolonged times could enhance the diffusion of the rejuvenator into the interface, consequently resulting in improved wettability. Moreover, by analyzing time-dependent changes in relation to the contact angle, Qin et al. [21] assessed the dynamic wettability of asphalt on aggregates and proposed that the utilization of a correlation function can effectively describe the wettability between asphalt and aggregates. Consequently, previous studies have shown that favorable wettability expands the bonding area of a CEACB on the RAP surface, expediting the interface fusion process and ultimately leading to increased bonding strength [7,22,23]. The quantitative characterization of the early wettability is crucial to the formation and development of the strength of the mixture.

Meanwhile, quantitative assessments of the bonding capacity between CEACB and RAP are of paramount significance in obtaining a deeper understanding of their formation and development behavior. Conventional techniques for evaluating bonding capacity, such as the boiling method [24], the shear test method [25], and the photoelectric colorimetric method [26], have been observed to possess certain constraints in terms of their application. Nevertheless, the binder bond strength (BBS) test has garnered significant attention owing to its objectivity and advantages in offering a direct, rapid, and precise evaluation [27]. Huang et al. [28] advocated the for the use of the BBS test as a superior method for assessing the bonding strength between asphalt and subgrade, emphasizing its heightened reliability in comparison to other testing approaches. Lu et al. [29] reaffirmed the efficacy and simplicity of utilizing the BBS test for efficiently determining the bond strength of asphalt binders. In an effort to further validate the effectiveness of the BBS test, Moraes et al. [30] compared its results with an enhanced dynamic shear rheometer strain sweep test, revealing that the BBS test demonstrated repeatability and reproducibility. Previous research has predominantly focused on the mechanical assessment of interfacial bonding strength; nevertheless, the influence of initial wettability on the ultimate interfacial bonding capacity between CEACB and RAP lacks systematic investigation. Therefore, conducting a comprehensive exploration with the perspective of the whole process of formation and development of interfacial bonding capacity is advantageous for comprehending the behaviors of strength evolution and failure of CRAEMs.

In addition, the analysis of interface failure patterns, including cohesive and adhesive failures, reflects the bonding capacity between CEACB and RAP to some extent. It is also significantly important to implement targeted measures to enhance the spall resistance performance of CRAEMs. With continual advancements in digital image processing (DIP) techniques, the quantification of image morphology has been widely applied in the field of road engineering to characterize and explain material features [31,32]. Ye et al. [33] and Yin et al. [34] employed quantitative image analysis to characterize the distribution of SBS in asphalt binders. Ye et al. [35] and Yuan et al. [36] used quantitative image analysis to reveal the effect of naphthenic oil as an additive on the structure of an SBS-modified asphalt binder. Rui et al. [37] found that digital imaging-assisted tests can greatly improve the assessment accuracy of hot-mix asphalt moisture damage. Alayat et al. [38] proposed a crack detection technique utilizing digital image processing in MATLAB, demonstrating its effectiveness in accurately estimating pavement dimensions and area, even under challenging surface conditions, by successfully eliminating undesired objects from the images. By employing digital image processing techniques, Yue et al. [32] conducted a quantitative analysis of the distribution, shape, and orientation of coarse aggregates in AC mixtures, which revealed that grading the cross-sectional area of aggregates based on Feret diameter reliably predicts the sieve grading of coarse aggregates used in AC mixtures. These studies have important reference value for quantifying the image results obtained from BBS experiments and identifying the interface failure patterns occurring between CEACB and RAP. Therefore, the application of innovative image processing techniques will be necessary to facilitate a comprehensive and precise evaluation of their bonding capacity.

As mentioned above, it is crucial to conduct a comprehensive exploration with the perspective of the whole formation and development process of interfacial bonding capacity. However, due to numerous influencing factors in construction, determining the extent of influence of each factor on material properties and making targeted improvements according to actual needs is challenging. Building upon the investigation of initial wettability behavior and quantifying the bonding capacity, this paper explores the influence of environmental parameters and the composition of CEACB on its ultimate bonding capacity. Specifically, this study aims to achieve the following:

(1) Reveal the dynamic wettability and spreading behavior of CEACB on RAP surfaces based on contact angle and surface free energy tests.
(2) Establish a visible evaluation method to explore the interfacial failure patterns between CEACB and RAP with the application of DIP.
(3) Conduct grey relational analysis to quantitatively evaluate the impact of cement content, curing temperature, and curing time on the ultimate interfacial bonding capacity.

This study contributes to enhancing the performance of CRAEMs and facilitating the widespread application of cold reclaimed asphalt pavement to fulfill sustainable development objectives.

2. Materials and Methods

2.1. Materials

Slow-setting cationic emulsified asphalt with a 60% solid content and ordinary Portland cement graded at 42.5 MPa (PO·42.5) were used to prepare the CEACB. Table 1 presents the essential properties of the emulsified asphalt, which were measured in accordance with several related ASTM specifications. The chemical composition analysis of the cement was conducted using an X-ray spectrometer (D8 Advance, Bruker AXS, Karlsruhe, Germany), and the results are provided in Table 2.

Table 1. The table shows the properties of the emulsified asphalt.

Properties	Unit	Value	Test Method
Test on Emulsified Asphalt			
Sieve test (1.18 mm)	%	0.01	ASTM D244 [39]
Storage stability (1 day, 25 °C)	%	0.4	ASTM D244
Storage stability (5 days, 25 °C)	%	3.2	ASTM D244
Test on Asphalt Residue			
Solid content	%	60.0	ASTM D244
Penetration (25 °C, 100 g, 5 s)	0.1 mm	75.3	ASTM D5 [40]
Ductility (25 °C)	cm	80.4	ASTM D113 [41]
Kinematic viscosity	Pa·s	95.2	ASTM D2170 [42]
Softening point	°C	49.5	ASTM D36 [43]

Table 2. The table shows the chemical composition of the cement.

Composition	Weight Percentage
CaO	61.13
SiO_2	24.48
Al_2O_3	5.05
MgO	2.33
SO_3	2.04
Fe_2O_3	3.38
K_2O_3	0.54
Na_2O	0.77
TiO_2	0.08

2.2. Samples Preparation

2.2.1. CEACB

While preparing CEACB, a blend of cement, emulsified asphalt, water, and a range of additives, including organic silicon defoamer and polycarboxylate superplasticizer, were employed to fulfill specific requirements [44]. The CEACB was established with asphalt-to-cement (A/C) mass ratios of 0.6, 1.0, and 1.4, respectively. To ensure uniform dispersion and eliminate bubbles, a defoamer was added at a concentration of 0.3%, along with the incorporation of a superplasticizer at a ratio of 2% relative to the total mass. The preparation process primarily includes the following steps: At first, the cement was slowly introduced and mixed at low speed for 30 s after thoroughly mixing additional water, defoamer, and superplasticizer. Subsequently, emulsified asphalt was introduced and agitated for 3 min at 120 rpm, followed by an additional 1 min mixing at 60 rpm to eliminate larger bubbles. After achieving uniform mixing of all components, the specimens were transferred to a humidity chamber set at a consistent temperature of 25 °C and a relative humidity of 65%.

2.2.2. Artificial RAP Substrate

The aged asphalt utilized for the experiments originated from the RAP of the Jinhua section within Zhejiang Province, China, which is part of the Shanghai–Kunming Expressway. This specific road segment had been in service for a duration exceeding eight years. An automatic asphalt analyzer (PAVELAB50, CONTROLS, Milan, Italy) was utilized to extract the RAP. Subsequently, the aging asphalt solution was recovered via the Abson method to obtain the aged asphalt.

For precise emulation of the RAP, a consistent and fine layer of aged asphalt film was meticulously applied to the surface of a basalt aggregate in this research. This procedure facilitated a direct evaluation of the bonding capacity between CEACB and RAP through the binder bond strength (BBS) test. The surface coating methodology used for the basalt aggregate involved the following steps:

(1) Select a smooth and uniform basalt substrate with a consistent surface roughness and ensure that the coating equipment is preheated to 135 °C.

(2) Heat the aged asphalt to 160 °C for complete fluidity assurance.
(3) Apply a small quantity of aged asphalt at a temperature of 135 °C onto a designated area, swiftly spreading it out using a scraper to form a uniform film over the surface of the basalt aggregate.
(4) The subsequent experiments were conducted using cooled product, allowing it to reach equilibrium with room temperature, as illustrated in Figure 1.

Figure 1. The figure shows the artificial RAP substrate.

2.3. Test Methods

2.3.1. Contact Angle Test

Optical contact angle apparatus (FCA2000A1, Shanghai, China) was utilized to assess the interfacial wetting properties between CEACB and RAP considering A/C ratios of 0.6, 1.0, and 1.4. During the measurements, CEACB was dropped onto the artificial RAP substrate using syringes, and the contact angle was recorded every two seconds over a 50 s duration. The optical contact angle apparatus is shown in Figure 2.

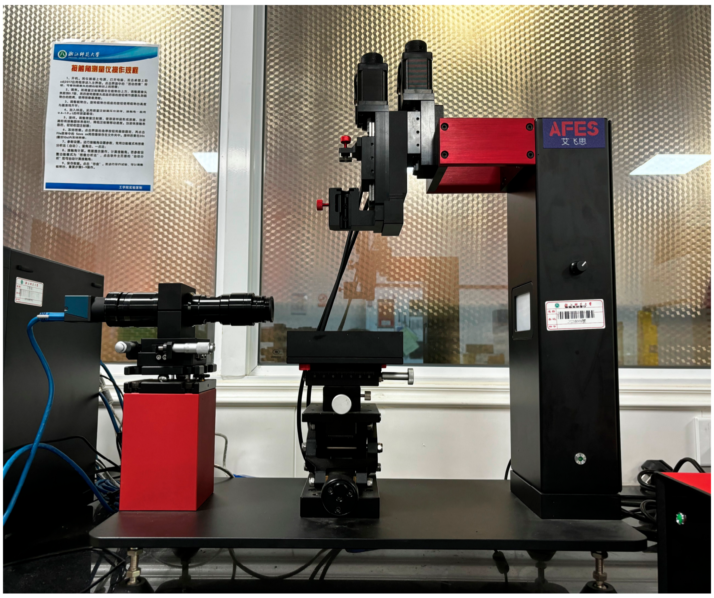

Figure 2. The figure shows the optical contact angle apparatus.

2.3.2. Binder Bond Strength Test

The assessment of the interfacial bonding strength between the CEACB and RAP was conducted using the binder bond strength (BBS) test, commonly referred to as the drawing test. The BBS test was conducted using automatic equipment (Posi Test AT-A, DeFelsko, West Chester, PA, USA), as illustrated in Figure 3.

Figure 3. The figure shows the PosiTest AT-A.

To account for the significant influence of the thickness of the asphalt film on the interface bonding force, a customized groove with a depth of 0.2 cm and a supporting ring with a bottom edge width of 1 mm were employed in this study. The test specimen consisted of a spindle with a uniformly rough surface at the bottom of the groove to ensure consistent asphalt distribution within it. The experimental principles of the BBS test equipment are visually depicted in Figure 4.

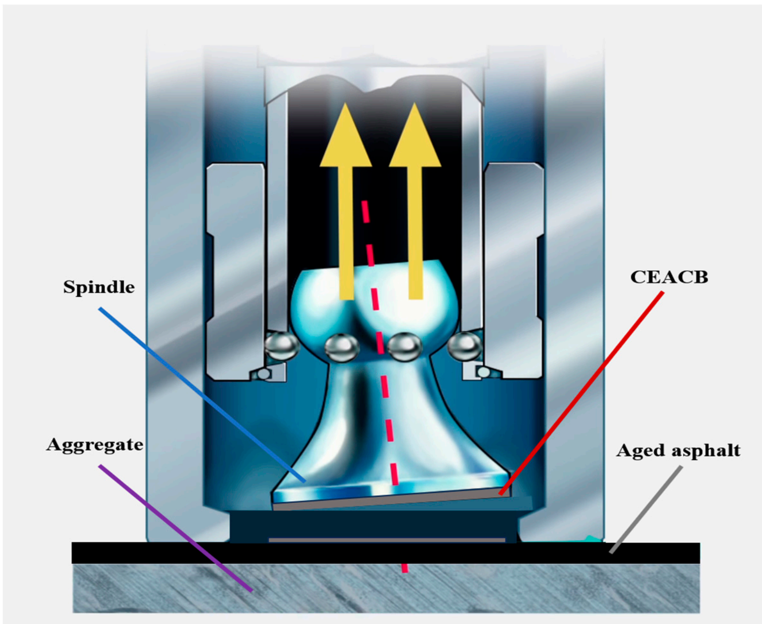

Figure 4. The figure shows the schematic configuration of BBS test.

The primary operational steps of the BBS test are listed as follows:

(1) Place silicone molds with a thickness of 2 mm and a diameter of 11 mm onto an artificial RAP substrate to stabilize it.
(2) Extract a sufficient amount of CAECB with different A/C ratios using droppers and evenly distribute them at the center of the silicone molds to form convex droplets. Swiftly position the heated spindles onto the CEACB confined within the silicone molds, adjust their positions to press into the molds, and eliminate any excess CEACB, as shown in Figure 5.
(3) Apply a uniform and constant load to the spindles using slates. Then, subject them to curing at temperatures of 25 °C and 40 °C for periods of 1 and 3 days, respectively.
(4) Draw out the samples after undergoing different curing temperatures and curing times. Attach the spindles to the drawing short column through adjustments, gradually applying tensile force to the spindles at a loading rate of 0.7 MPa/s. Continuously monitor changes in the display and image until failure occurs. The failure pressure measurements are converted into Pull-Off Tensile Strength (POTS) for record-keeping purposes. The POTS is calculated based on the maximum display load, instrument calibration data, and original stress surface area.

(**a**) (**b**) (**c**)

Figure 5. The figure shows the (**a**) pull-off stub, (**b**) specimen, and (**c**) samples of BBS test.

2.4. Theoretical Methods

2.4.1. Surface Free Energy

Surface free energy is a parameter that characterizes the interaction between a solid surface and a liquid, emphasizing the wetting and bonding tendencies of the liquid towards the solid surface. During the bonding process between CEACB and artificial RAP substrate, there exists a three-phase contact involving the liquid, gas, and solid, resulting in the elimination of individual gas–liquid and gas–solid interfaces while giving rise to a unified solid–liquid interface.

The quantitative evaluation of the mutual attraction between the liquid and solid, as well as the wetting of the liquid on the solid surface, can be determined by calculating ΔG (negative change in surface free energy) at this interface segment, as expressed in Equation (1).

$$\Delta G = \gamma_{s-g} + \gamma_{l-g} - \gamma_{s-l} \tag{1}$$

where ΔG represents the change in surface free energy at the liquid–solid interface, γ_{s-l} represents the solid–liquid surface free energy, γ_{l-g} represents the liquid–gas surface free energy, and γ_{s-g} represents the solid–gas surface free energy. The intuitive distribution of variables is shown in Figure 6.

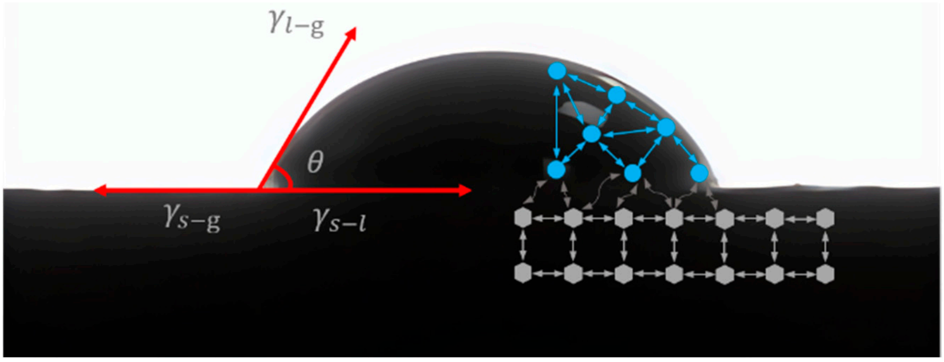

Figure 6. The figure shows the variables of Young's Equation using contact angle.

In liquid substances, surface energy is often used interchangeably with surface tension. Although there are subtle distinctions between surface energy and surface tension according to the theory of thermodynamics, in practical usage, these terms are frequently utilized synonymously [45].

By substituting Young's equation [46,47] (Equation (2)) into the calculation, Equation (3) is obtained, which indicates that calculating ΔG requires the determination of both the surface tension of CEACB and the contact angle between CEACB and the artificial RAP substrate:

$$\gamma_{s-g} - \gamma_{s-l} = \gamma_{l-g} cos\theta \tag{2}$$

$$\Delta G = \gamma_{l-g}(1 + cos\theta) \tag{3}$$

where $cos\theta$ represents the contact angle formed between a liquid droplet and a solid surface.

The surface tension of CEACB was measured using the pendant drop method. An injector needle with an outside diameter of 0.8 mm was employed to generate a pendant drop, which experienced deformation as the drop weight increased. The resulting droplet state image was captured using optical contact angle apparatus and analyzed with CAD (2016) software to obtain the necessary data for surface tension calculation based on Young's equation (Equation (2)). Both schematic and experimental illustrations of this process are depicted in Figure 7.

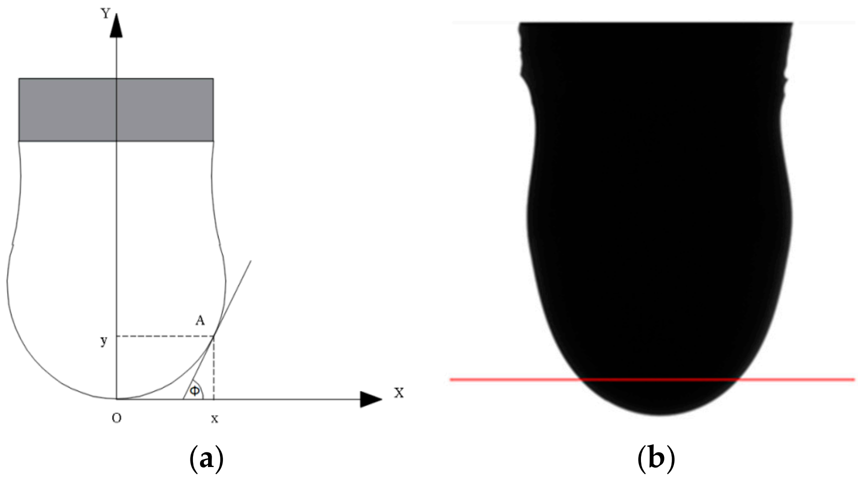

Figure 7. The figure shows a (**a**) schematic diagram of the pendant drop method and (**b**) an image of a drop.

Utilizing the Young–Laplace equation and establishing a correlation between pressure variance inside and outside a droplet, surface tension, and curvature radius, CEACB droplets can be precisely positioned at the tip of a capillary tube and arranged in symmetrical two-dimensional coordinates about the Y-axis. The lower part of the droplet is tangential to the X-axis, while its shape can be accurately characterized by the coordinates A(x,y) on the plane.

When the gravity of a droplet is balanced by its surface tension, the following equilibrium equation can be obtained, as shown in Equation (4):

$$\Delta P_o - \Delta P_A = \Delta\rho \cdot g \cdot y \tag{4}$$

where ΔP_o represents the pressure differential between inside and outside the droplet at vertex O, ΔP_A represents the pressure difference inside and outside the droplet at point A, and g is the acceleration of gravity, taken as 9.8 m/s^2; assuming that the droplet contour is symmetric about the Y-axis, the curvature at vertex O is isotropic. By combining Equation (4) and analyzing the curvature of point A (x, y) geometrically, the following Equation (5) can be obtained:

$$\frac{d\varphi}{dl} = 2k_o - \frac{y \cdot \Delta\rho \cdot g}{\gamma_{l-g}} - \frac{sin\varphi}{x} \tag{5}$$

where k_o is the curvature at vertex O, l is the arc length of the droplet contour, φ is the angle between the tangent line at point A and the X-axis, x and y are coordinate values, $\Delta\rho$ is the density difference, uniformly approximated as 0.39 kg/m^3, and γ_{l-g} is the surface tension.

In order to better solve the problem, x, y, l, and k_o are all defined in non-dimensional forms, as illustrated in Equation (6).

$$X = \frac{x}{a}; Y = \frac{y}{a}; L = \frac{l}{a}; B = \frac{1}{a \cdot k_o}; a = \sqrt{\frac{\gamma_{l-g}}{\Delta\rho \cdot g}} \tag{6}$$

Since $X = Y = L = \varphi = 0$ at vertex O, the following can be obtained:

$$\frac{sin\varphi}{x} = \frac{1}{B} \tag{7}$$

By Equation (6), the following can be obtained:

$$\gamma_{l-g} = a^2 \cdot \Delta\rho \cdot g;\ a = \frac{1}{B \cdot k_o} \tag{8}$$

By Equation (7), the following can be obtained:

$$B = \frac{x}{sin\varphi} \tag{9}$$

By combining Equations (8) and (9), the surface tension calculation formula can be obtained as follows:

$$\gamma_{l-g} = \frac{(sin\varphi)^2}{x^2 \cdot {k_o}^2} \cdot \Delta\rho \cdot g = \frac{(sin\varphi)^2 \cdot {R_o}^2}{x^2} \cdot \Delta\rho \cdot g \tag{10}$$

By employing CAD software to analyze the images, the radius of curvature R_o, angle φ, and intercept x of the cement emulsified asphalt composite binder fluid with different A/C ratios can be obtained. Substituting these values into Equation (8) enables the calculation of the surface tension.

2.4.2. Grey Relational Analysis

Grey relational analysis (GRA) was employed to investigate the wettability of CEACB before curing and its correlation with environmental factors during the curing process, as well as its influence on the bonding capacity between CEACB and the artificial RAP substrate. GRA proves to be a robust methodology for analyzing intricate relationships among multiple parameters. The analysis comprises three main stages: data pre-processing, the computation of grey relational coefficients, and the derivation of grey relational grades.

Consider $x_0^{(0)}(k)$ as the reference sequence and $x_i^{(0)}(k)$ as the comparative sequence within the framework of GRA. Equation (11) mathematically represents the original data series $X^{(0)}(k)$.

$$\mathrm{X}^{(0)}(k) = \begin{bmatrix} x_0^{(0)}(k) \\ x_i^{(0)}(k) \end{bmatrix} = \begin{bmatrix} x_0^{(0)}(1) & x_0^{(0)}(2) & \cdots & x_0^{(0)}(n) \\ x_1^{(0)}(1) & x_1^{(0)}(2) & \cdots & x_1^{(0)}(n) \\ x_2^{(0)}(1) & x_2^{(0)}(2) & \cdots & x_2^{(0)}(n) \\ \vdots & \vdots & \vdots & \vdots \\ x_m^{(0)}(1) & x_m^{(0)}(2) & \cdots & x_m^{(0)}(n) \end{bmatrix} \tag{11}$$

where i ranges from 1 to m, representing the factors, and k ranges from 1 to n, representing the data items.

(1) Data pre-processing

The original sequences underwent data pre-processing to standardize them for comparative analysis. In this study, a widely accepted normalization approach was utilized, which involves dividing each value in the original sequence by its initial value. This normalization process is illustrated in Equations (12) and (13).

$$x_0^* = \frac{x_0^{(0)}(k)}{x_0^{(0)}(1)} \tag{12}$$

$$x_i^* = \frac{x_i^{(0)}(k)}{x_i^{(0)}(1)} \tag{13}$$

where x_0^* represents the reference sequences and x_i^* signifies the comparative sequences post data pre-processing.

(2) Grey relational coefficient

After completing data pre-processing, grey relational coefficients are computed from the normalized sequences to evaluate the correlation between the reference and comparative sequences. The computation of the grey relational coefficient is performed using Equation (14):

$$\gamma_{0i}(k) = \frac{\Delta_{min} + \xi\Delta_{max}}{\Delta_{0i}(k) + \xi\Delta_{max}} \tag{14}$$

where $\gamma_{0i}(k)$ represents the grey relational coefficient between $x_0^*(k)$ and $x_i^*(k)$. $\Delta_{0i}(k)$ denotes the deviation sequence of $x_0^*(k)$ and $x_i^*(k)$, which is computed as $\Delta_{0i}(k) = \left|x_0^*(k) - x_i^*(k)\right|$. Additionally, Δ_{min} stands for the minimum value of $\Delta_{0i}(k)$ across all i and k, while Δ_{max} signifies the maximum value of $\Delta_{0i}(k)$ across all i and k. The distinguishing coefficient ξ, often set at 0.5, falls within the range of $|0, 1|$.

(3) Grey relational grade

After calculating the grey relational coefficient, the resulting grey relational grade Γ_{0i} is computed using Equation (15). A higher value of this grade indicates a stronger correlation between the reference sequence and its respective comparative sequence.

$$\Gamma_{0i} = \frac{1}{n}\sum_{k=1}^{n} \gamma_{0i}(k) \tag{15}$$

3. Results and Discussion

3.1. Initial Wettability of CEACB on RAP Surface

3.1.1. Initial Wettability Analysis Based on Contact Angle

The evolution of the contact angle over time between the emulsified asphalt, three distinct groups of CEACBs with varying A/C ratios, and the aged asphalt film on the artificial RAP surface is illustrated in Figure 8. As time progresses, there is a gradual and consistent decrease in the contact angle between the emulsified asphalt and the surface of the artificial RAP substrate, eventually reaching equilibrium. However, stage characteristics can be observed in the variations of contact angles between the CEACBs and the artificial RAP substrate:

(1) Rapid wetting stage (0–5 s): during this initial stage, the contact angle of the CEACBs with varying A/C ratios exhibited a rapid decrease.
(2) Gradual wetting stage (5–35 s): subsequently, the rate of contact angle reduction slows down, and the curve tends to flatten.
(3) Equilibrium wetting stage (beyond 35 s): in the final stage, the contact angle continued to decrease extremely slowly until reaching an equilibrium value, typically occurring around 45 s.

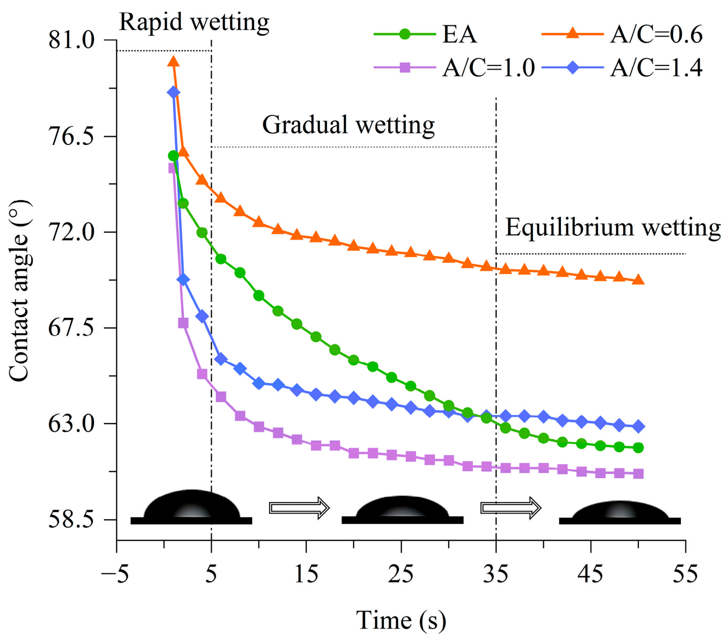

Figure 8. The figure shows the contact angle in time dimension.

The results indicate that the addition of cement significantly affects the initial wettability of CEACBs, showing distinct phase characteristics compared to emulsified asphalt. For CEACBs, during the initial wetting stage, the incorporation of cement reduces their surface tension, leading to a notable decrease in the contact angle and facilitating rapid wetting and diffusion. As the duration of wetting increases, the change in contact angle gradually decreases, indicating a trend toward stability in the interaction between cement and emulsified asphalt. Eventually, with continuous wetting, the contact angle progressively decreases until it reaches an equilibrium state resembling Young's contact angle. The overall impact on the wettability of CEACB is influenced by various factors, such as cement hydration heat release, the generation of hydration products, and the interaction between cement and asphalt.

Comparing the variations in the contact angles of CEACBs under three different A/C ratios reveals that the CEACBs demonstrate the highest contact angles at an A/C ratio of 0.6, followed by 1.4 and 1.0, respectively. At an A/C ratio of 0.6, the CEACB exhibits a significantly larger contact angle compared to that of the emulsified asphalt. Excessive cement content can lead to the partial agglomeration of cement particles, hinder cement hydration, reduce the flowability of CEACBs, and result in unfavorable wetting effects. When the A/C ratio is 1.4, the contact angle between the CEACB and emulsified asphalt approaches equilibrium around 35 s following their intersection. A lower cement content makes its surface susceptible to being enveloped by the demulsified asphalt, leading to a certain degree of inhibition in terms of hydration reaction. Under an A/C ratio of 1.0, it was observed that the contact angle for CEACB consistently remained lower than that of emulsified asphalt, which indicates that maintaining an appropriate level of cement content promotes favorable interactions between cement and emulsion. This process accelerates heat release during cement hydration, while concurrently reducing the surface tension of CEACB and resulting in a more significant reduction in contact angle.

To further evaluate the influence of cement content on the dynamic wettability of CEACB on the aged asphalt film surface, logarithmic transformation was applied to three sets of CEACB contact angles, followed by function fitting. The fitting results are presented in Figure 9 using the linear function form $Y = kX + b$, where parameter 'b' signifies the initial contact angle of CEACB on the aged asphalt surface, and parameter 'k' reflects the rate of change in the contact angle [21]. The absolute value of 'k' is used to represent the diffusion coefficient, with a larger coefficient indicating a faster wetting speed. The correlation coefficient R^2 was employed as an indicator to evaluate fitting quality, with values closer to 1 signifying higher accuracy in fitting. All three sets of fitted functions exhibit a correlation coefficient exceeding 0.85, showcasing the model's capability to precisely assess the rate at which CEACB's contact angle varies during wettability on the aged asphalt surfaces.

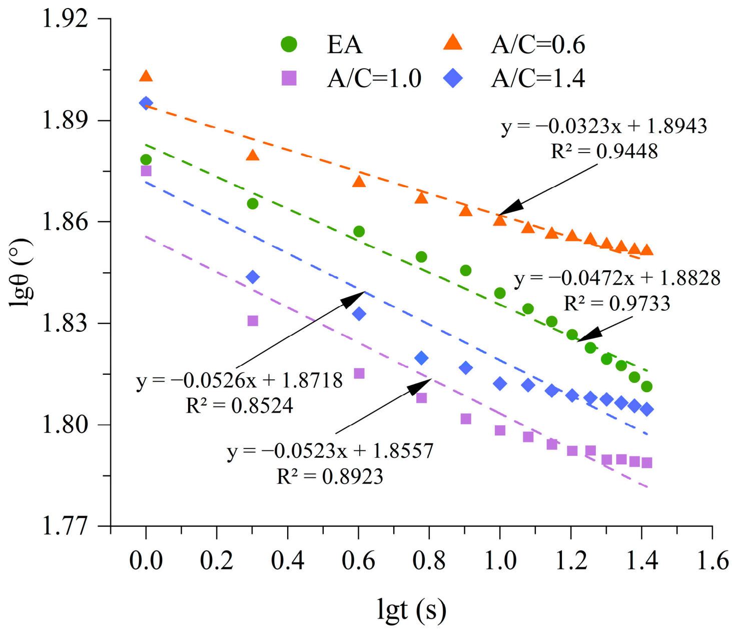

Figure 9. The figure shows the spreading behavior of the CEACBs.

As shown in Figure 9, the diffusion coefficients of CEACBs at the A/C ratios of 1.4 and 1.0 are 0.0526 and 0.0523, respectively, ranking first and second. This indicates a higher rate of change in contact angle and improved wettability and spreading behavior of CEACBs on the aged asphalt surface. When the A/C ratio is 0.6, the diffusion coefficient reaches its minimum value of only 0.0323, which is lower than that of pure emulsified asphalt (0.0472). This suggests that excessive cement content can lead to the partial agglomeration of cement particles, hindering hydration reactions. Additionally, inadequate heat generation from hydration also hampers the demulsification process of emulsified asphalt, further leading to a decrease in the wetting rate. Although the diffusion coefficient is slightly higher at an A/C ratio of 1.4 compared to 1.0, it is evident from the aforementioned analysis that wettability evaluation should encompass not only the rate of change in contact angle but also consider the contact angle sizes of the initial and spreading processes. The fitting function generally surpasses that seen at an A/C ratio of 1.0 when considering an A/C ratio of 1.4, indicating a larger overall contact angle. This phenomenon can be attributed to demulsified asphalt partially covering cement when its content is low, impeding cement hydration reactions and reducing heat production, consequently resulting in a greater overall contact angle. In summary, in this study, under suitable cement content conditions and with the investigated A/C ratio of 1.0, a significant enhancement is observed in the interaction between emulsified asphalt demulsification and cement hydration, resulting in an increase in heat release. This phenomenon significantly contributes to improving the wetting and spreading performance between CEACB and RAP.

Additionally, CEACB is a composite material composed of organic asphalt and inorganic cement, which exhibits distinctive viscoelastic properties that result in contact angle hysteresis on the surface of the aged asphalt film. To ensure experimental accuracy, it is crucial to measure the equilibrium contact angle of a CEACB on an aged asphalt surface. Table 3 provides the average value and coefficient of variation (CV) of the equilibrium contact angle of emulsified asphalt and three CEACBs. It is evident that at A/C ratios of 0.6 and 1.4, the equilibrium contact angle of CEACB exceeds that of emulsified asphalt. Conversely, at an A/C ratio of 1.0, the equilibrium contact angle of the CEACB is lower than that of the emulsified asphalt. Notably, at an A/C ratio of 1.0, the equilibrium contact angle reaches its minimum value for CEACB, indicating optimal wettability. These results are consistent with the dynamic wettability and spreading behavior of the CEACB shown in Figure 8.

Table 3. The tables shows the equilibrium contact angle.

A/C	Average Value (°)	CV (%)
EA	61.87	0.44%
0.6	69.70	1.09%
1.0	60.68	0.87%
1.4	62.88	1.34%

3.1.2. Initial Wettability Analysis Based on Surface Free Energy

Surface free energy is used as an indicator to quantify the initial wettability of a CEACB, and Formulas (1)–(10) are used for its calculation. The parameters in the calculation process and the calculation results are shown in Table 4. A smaller surface free energy value represents better wettability. The hydration reaction of cement releases heat, thereby increasing the energy of the molecules at the surface layer of the CEACB, potentially leading to a reduction in surface free energy. Simultaneously, the dissolution of inorganic salts generated from cement hydration in water may elevate the surface free energy of CEACB. However, despite the potential increase in surface free energy due to the formation of hydration products from cement, temperature remains as the predominant influencing factor. The addition of cement may lead to a decrease in the surface free energy of CEACB. Moreover, with an increase in cement content, there is a gradual diminishing effect in terms of the changes observed in the surface free energy of the CEACBs.

Table 4. The table shows the surface free energy and ΔG of CEACBs with RAP.

A/C	x (m)	φ (°)	Ro (m)	Surface Free Energy (mJ·m^{-2})	ΔG (mJ·m^{-2})
EA	7.362×10^{-3}	64.237	8.337×10^{-3}	3.975	5.849
0.6	6.689×10^{-3}	54.201	8.236×10^{-3}	3.812	5.135
1.0	6.277×10^{-3}	49.023	8.325×10^{-3}	3.831	5.707
1.4	7.247×10^{-3}	57.211	8.162×10^{-3}	3.426	4.988

At an A/C ratio of 1.4, the surface free energy of the CEACB significantly decreases due to an excessive coating of demulsified asphalt around cement particles, forming an obstructive asphalt film that hinders the dispersion of cement hydration products in water. Consequently, it intensifies the influence of temperature elevation on the surface free energy of CEACBs. At A/C ratios of 0.6 and 1.0, the measured surface free energies were found to be 3.812 $mJ \cdot m^{-2}$ and 3.831 $mJ \cdot m^{-2}$, respectively, with a slightly lower value observed at A/C = 0.6 owing to a higher cement content, which leads to cement agglomeration and incomplete cement hydration. Furthermore, calculations indicate that CEACBs exhibit the maximum ΔG at A/C = 1.0, signifying the highest energy required for detaching CEACBs from the surface of RAP and suggesting optimal adhesive performance.

3.2. Bonding Capacity between CEACB and RAP

3.2.1. Bonding Strength Evaluation Based on BBS

Figure 10 illustrates the POTS results obtained from BBS testing. POTS significantly increases with increased curing temperature and prolonged curing time. At standard room temperature (25 °C), whether cured for one day or three days, POTS reaches its maximum at A/C = 1.0. The same trend is observed at a curing temperature of 40 degrees, emphasizing the effectiveness of an appropriate A/C ratio in enhancing the interaction between cement and emulsified asphalt. This promotes the formation of a denser spatial network structure, thereby strengthening the interfacial bonding capacity between CEACBs and RAP.

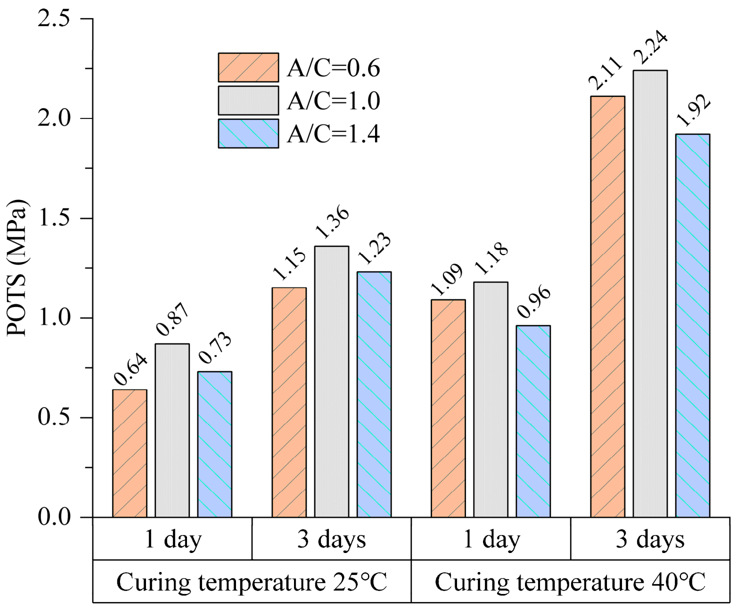

Figure 10. The figure shows POTS under different curing conditions.

It is noteworthy that the analysis of the growth rate of POTS concerning time and temperature reveals that, at a curing temperature of 25 °C, extending the curing time from 1 day to 3 days results in a modest increase of approximately 0.5 MPa in strength. However, at a higher curing temperature of 40 °C, the strength experiences a more significant gain of nearly 1 MPa over the same 1 to 3-day curing period. This substantiates that an optimal curing temperature significantly contributes to the formation of bonding strength. In instances of lower temperatures, extending the curing time becomes imperative to attain the desired strength. Conversely, higher temperatures reduce the required curing time, enabling the swift restoration of traffic access.

3.2.2. Failure Patterns Evaluation Based on DIP

The interface images obtained from the BBS test were captured using a digital camera. Due to the discrepancy in chromatic lateral aberration between CEACB and the aged asphalt film, the utilization of Halcon (12.0) machine vision software for gray binarization analysis of the interface image significantly contributed to refining the evaluation index for interface failure and improving the assessment of the bonding capacity between the CEACBs and RAP.

By implementing grayscale manipulation, the spalling ratio of CEACBs on the surface of the aged asphalt was quantified. This approach offers several advantages, including minimal errors and enhanced result reliability. The operational procedures are visually presented in Figure 11, encompassing a series of detailed steps:

(1) Employing a high-resolution camera to capture vertical images of the interfacial failure between a CEACB and artificial RAP substrate, ensuring consistent light intensity for accurate analysis.
(2) Undergoing pre-processing procedures involving clipping and noise reduction, the captured image was then transferred to Halcon software for channel conversion, thereby transforming the color channel into a monochrome channel.
(3) Executing channel conversion and implementing gray binarization, the CEACB was distinguished from the aged asphalt film with a distinct color gamut. Subsequently, the calculation of the pixel value ratio of the exposed aged asphalt film to the entire interface was then performed to establish the spalling rate index of cement-emulsified asphalt on the aged asphalt.

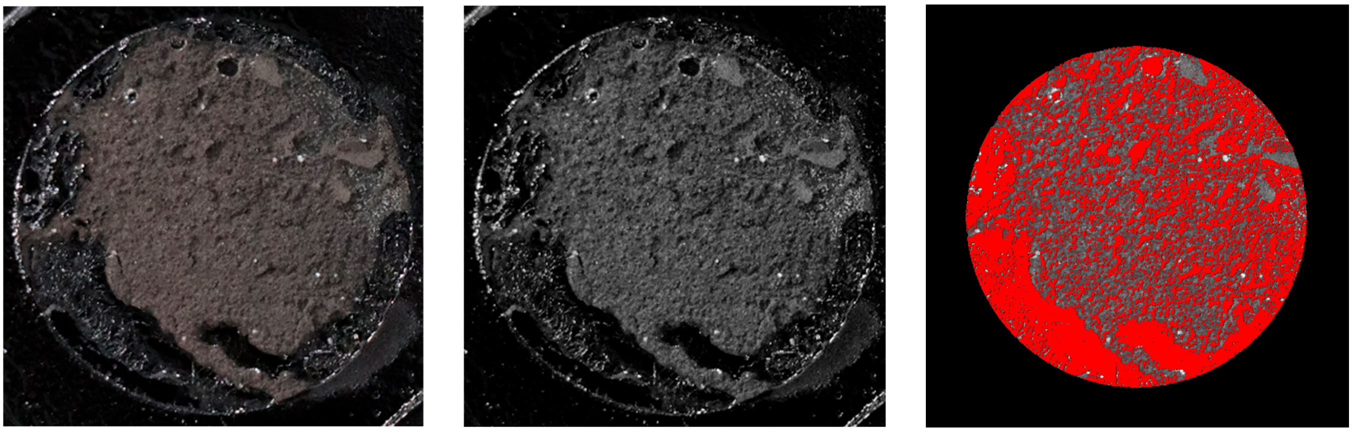

(**a**) (**b**) (**c**)

Figure 11. The figure shows the image analysis process of failure interface: (**a**) initial image, (**b**) single processing channel, and (**c**) binarization processing.

The differentiation between the CEACB and the aged asphalt was achieved by utilizing a distinct color gamut. The index for the spalling rate of CEACB from the artificial RAP substrate was determined by calculating the ratio between the pixel values of the exposed aged asphalt and the entire interface. Set the pixel value of the exposed aged asphalt to PIX_{age} and the pixel value of the entire damaged interface to $\mathrm{PIX}_{complete}$, then the spalling rate is equal to $\frac{PIX_{age}}{PIX_{complete}}$. A decreased spalling rate indicates more robust adhesion between the CEACB and the aged asphalt. This measurement aims to characterize the damage patterns between the CEACB and RAP, where a lower spalling rate signifies stronger adhesion between the CEACB and the aged asphalt. Twelve coated samples were prepared, and their respective test outcomes are outlined in Table 5.

As shown in Table 5, the CEACB spalling rates consistently decrease with increasing temperature across different A/C ratios. It is suggested that appropriately increasing the temperature contributes to the development of adhesion between a CEACB and RAP, thereby resulting in a decreased spalling rate. Moreover, it is noteworthy that the CEACB cured for 3 days exhibited significantly lower spalling rates compared to those cured for only 1 day under the same A/C ratio and curing temperature conditions. The reduction in the spalling rate is most pronounced at an A/C ratio of 1.0, followed by the A/C ratio of

1.4. Prolonging the curing time contributes to enhancing the interfacial bonding capacity between the CEACB and RAP, particularly demonstrating optimal adhesive strength at an A/C ratio of 1.0.

Table 5. The table shows the spalling rates analysis of failure interface.

Curing Temperature	Curing Time	A/C	0.6	1.0	1.4
25 °C	1 day	Spalling rate	0.435801	0.410952	0.459995
		Figures	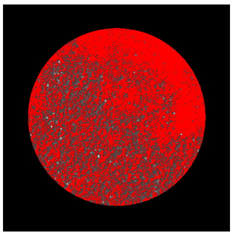	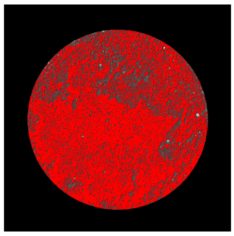	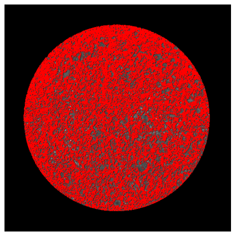
	3 days	Spalling rate	0.430479	0.390900	0.428894
		Figures	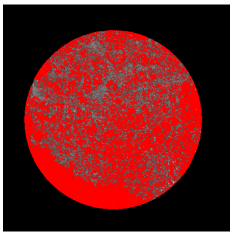	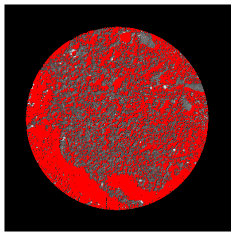	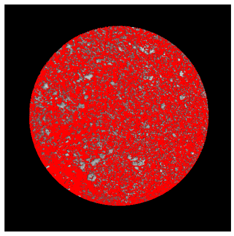
40 °C	1 day	Spalling rate	0.357687	0.349914	0.367774
		Figures	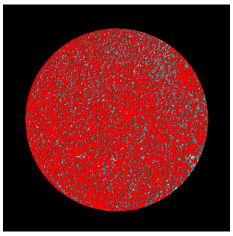	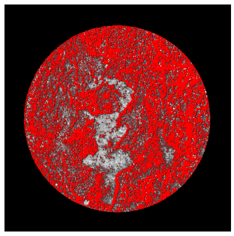	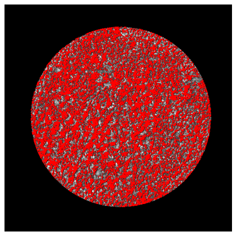
	3 days	Spalling rate	0.288313	0.231372	0.35768
		Figures	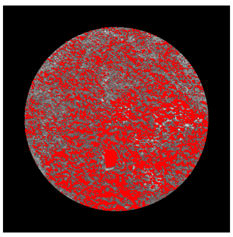	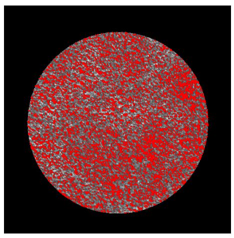	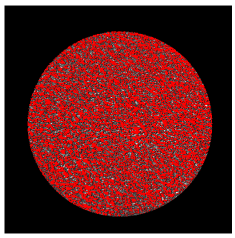

3.3. Grey Relational Analysis

The initial wetting condition of the CEACB on the RAP surface significantly impacts the ultimate interfacial bonding capacity between the CEACB and RAP. Optimal wetting conditions can accelerate and improve the coating of CEACB on RAP, thereby benefiting the coverage of emulsified asphalt on aggregates. The interaction between cement and RAP enhancers the bonding capacity at the interface, thereby improving the overall strength of CRAEMs. Furthermore, critical factors, such as cement content, curing time, and curing temperature exert a significant influence on the interfacial bonding capacity between CEACBs and RAP. To quantitatively assess the impact of these influencing factors on bonding capacity, this study utilized varying cement contents, curing times, and curing temperatures as comparative sequences while considering their effects on wettability and strength development processes. Subsequently, a comprehensive grey relational analysis was conducted using maximum POTS and spalling rate as reference sequences. The detailed initial sequence is provided in Table 6. The grey relational grades calculated using Equations (10)–(15) are displayed in Figure 12.

Table 6. The table shows the original data series of the grey relational analysis (GRA).

Number	Comparative Sequences			Reference Sequences	
	Cement Content (A/C)	Curing Time (day)	Curing Temperature (°C)	Artificial RAP Substrate	
				POTS (Mpa)	Spalling Rate (%)
1	0.6	1	25	0.64	43.58
2	0.6	1	40	1.09	35.77
3	0.6	3	25	1.15	43.05
4	0.6	3	40	2.11	28.83
5	1.0	1	25	0.87	41.10
6	1.0	1	40	1.81	34.99
7	1.0	3	25	1.36	39.09
8	1.0	3	40	2.24	23.14
9	1.4	1	25	0.73	46.00
10	1.4	1	40	0.96	36.78
11	1.4	3	25	1.23	42.89
12	1.4	3	40	1.92	35.77

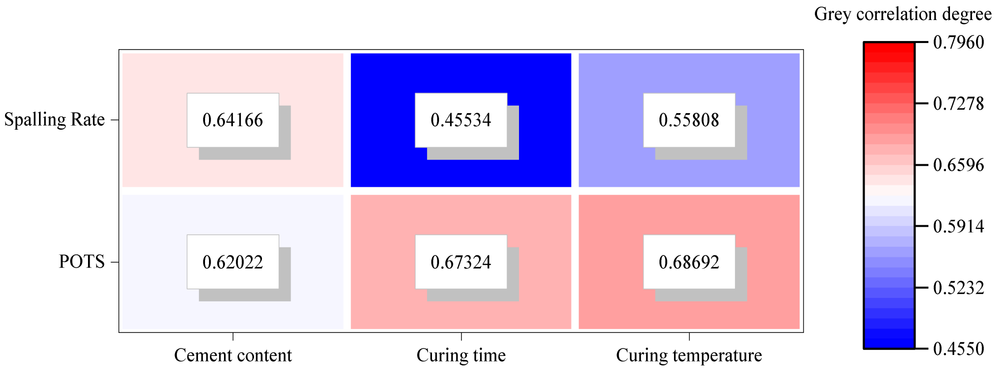

Figure 12. The figure shows grey relational degree.

When utilizing the POTS as the reference sequence, the GRA reveals a high correlation between curing temperature and curing time, with respective relational degrees of 0.68692 and 0.67324. The curing temperature influences the POTS by regulating both the chemical reactions and structure formation of CEACBs during the curing process. Higher curing temperature accelerates cement hydration reactions and the demulsification of emulsified asphalt, thereby improving CEACB strength. Curing time represents the duration of CEACB solidification, and prolonging this duration notably enhances the strength and structural integrity of CEACBs. As the cement hydration reaction progresses, there is an increased production of hydration products and crystalline substances that interact with the emulsified asphalt, thereby further reinforcing the bonding strength between the CEACB and RAP.

When utilizing the spalling rate as the reference sequence, the highest correlation is found with cement content, at 0.64166. The wettability of a CEACB is intricately affected by the cement content through modifications in the viscosity, flow properties, particle size distribution, and chemical interactions. The results demonstrate that favorable wettability increases the contact area between a CEACB and RAP, facilitating more effective infiltration of the CEACB into the RAP surface. Consequently, this enhances the interfacial adhesion between the CEACB and RAP, thereby reducing the possibility of spalling occurrence.

However, there is a less pronounced association between curing time, curing temperature, and spalling rate, particularly noteworthy is the fact that the correlation degree between curing time and spalling rate is less than 0.5, which significantly deviates from correlations observed with the other influencing factors. These findings indicate that wettability primarily influences the spalling rate at the interface between a CEACB and RAP. Meanwhile, the establishment of bonding capacity between an CEACB and RAP surface is not yet fully formed, thereby limiting the influence of curing time on the spalling rate. Nevertheless, over time, the extent of CEACB curing intensifies, and the impact of curing time on the spalling rate becomes increasingly apparent, particularly during the later stages of curing.

Ensuring the optimal performance of CRAEMs in road construction is crucial and requires a comprehensive consideration of multiple key factors in practical engineering. Firstly, curing temperature stands as a critical parameter. Elevating the curing temperature accelerates cement hydration reactions and the emulsified asphalt demulsification process, thereby promoting rapid curing and structural formation of CEACBs. Secondly, it is necessary to reasonably schedule the curing time. Prolonging the curing time fosters internal reactions and promotes strength development within the CRAEM. However, achieving a balance between road closure duration and curing time is essential to ensure prompt road opening while preserving the performance integrity of CRAEMs. Thirdly, exercising control over cement content helps to optimize the initial wettability of CEACBs, which significantly mitigating the risk of spalling failure of asphalt pavement. Therefore, meticulous design of material formulations and construction parameters is crucial in practical engineering to ensure reliable quality and strength of CRAEMs.

4. Conclusions

The whole process of strength development and failure between CEACBs and RAP was systematically investigated, according to the surface energy theory combined with the correlation analysis between initial wettability and ultimate bonding capacity. The primary conclusions are summarized as follows:

(1) The wettability and spreading behavior of CEACBs on the aggregate surface were successfully characterized via contact angle measurements and subsequent function fitting. The wettability of CEACBs on the aggregate surface initially increases and subsequently decreases with increasing cement content, suggesting a positive influence of appropriate cement content on the wettability of CEACBs on RAP.

(2) The incorporation of BBS test and image processing technology enhances reliability in recognizing failure patterns. By properly prolonging the curing time and controlling the curing temperature, significant improvements can be achieved in the bonding capacity of CEACBs, resulting in higher drawing force between CEACBs and RAP. Cohesive failure patterns within CEACBs become more predominant.

(3) In the cementation process between CEACBs and RAP, an obvious correlation is observed between initial wettability and ultimate bonding capacity. Notably, the wettability of CEACBs exerts the most significant influence on the initial formation of interface strength, especially on the spalling rate. Conversely, the effects of curing time and curing temperature on this process are relatively minor.

(4) Based on the analysis of grey correlation degree, it can be concluded that the optimization of material ratio should be emphasized in the engineering practice, which is conducive to effectively enhancing the interfacial bonding capacity of asphalt mixtures and improving the initial strength and anti-spalling ability of asphalt pavement.

Author Contributions: Conceptualization, K.Z.; Data curation, X.Q. and Z.C.; Formal analysis, K.Z. and Q.Y.; Investigation, Q.Y., X.Q. and W.X.; Project administration, W.X.; Software, W.X.; Supervision, K.Z.; Validation, Q.Y. and X.Q.; Writing—original draft, Q.Y.; Writing—review and editing, K.Z., W.X., H.L. and Z.C. All authors have read and agreed to the published version of the manuscript.

Funding: This research was funded by the Natural Science Foundation of Zhejiang Province [grant numbers LY23E080002, LY21E080011] and the Science and Technology Plan Project of Jinhua Technology Bureau [grant numbers 2021-3-175, 2022-3-072].

Data Availability Statement: Data will be made available upon request.

Acknowledgments: The authors are great grateful for the assistance from Zile He in conducting the experiments for this paper.

Conflicts of Interest: The authors declare no conflicts of interest.

References

1. Wang, J.; Yuan, J.; Xiao, F.; Li, Z.; Wang, J.; Xu, Z. Performance investigation and sustainability evaluation of multiple-polymer asphalt mixtures in airfield pavement. *J. Clean. Prod.* **2018**, *189*, 67–77. [CrossRef]
2. Gao, L.; Ni, F.; Charmot, S.; Luo, H. Influence on Compaction of Cold Recycled Mixes with Emulsions Using the Superpave Gyratory Compaction. *J. Mater. Civ. Eng.* **2014**, *26*, 04014081. [CrossRef]
3. Lambert, M.; Piau, J.-M.; Gaudefroy, V.; Millien, A.; Dubois, F.; Petit, C.; Chaignon, F. Modeling of cold mix asphalt evolutive behaviour based on nonlinear viscoelastic spectral decomposition. *Constr. Build. Mater.* **2018**, *173*, 403–410. [CrossRef]
4. Sangiorgi, C.; Tataranni, P.; Simone, A.; Vignali, V.; Lantieri, C.; Dondi, G. A laboratory and filed evaluation of Cold Recycled Mixture for base layer entirely made with Reclaimed Asphalt Pavement. *Constr. Build. Mater.* **2017**, *138*, 232–239. [CrossRef]
5. Gao, J.; Yang, J.; Yu, D.; Jiang, Y.; Ruan, K.; Tao, W.; Sun, C.; Luo, L. Reducing the variability of multi-source reclaimed asphalt pavement materials: A practice in China. *Constr. Build. Mater.* **2021**, *278*, 122389. [CrossRef]
6. Yang, J.; Tao, W.; Gao, J.; Yu, D.; Zhou, J.; He, L.; Yao, Y. Measurement of particle agglomeration and aggregate breakdown of reclaimed asphalt pavement. *Constr. Build. Mater.* **2021**, *296*, 123681. [CrossRef]
7. Wang, Z.; Wang, P.; Guo, H.; Wang, X.; Li, G. Adhesion Improvement between RAP and Emulsified Asphalt by Modifying the Surface Characteristics of RAP. *Adv. Mater. Sci. Eng.* **2020**, *2020*, 4545971. [CrossRef]
8. Fang, X.; Garcia-Hernandez, A.; Lura, P. Overview on Cold Cement Bitumen Emulsion Asphalt. *RILEM Tech. Lett.* **2016**, *1*, 116–121. [CrossRef]
9. Oruc, S.; Celik, F.; Akpinar, M.V. Effect of Cement on Emulsified Asphalt Mixtures. *J. Mater. Eng. Perform.* **2007**, *16*, 578–583. [CrossRef]
10. Rutherford, T.; Wang, Z.; Shu, X.; Huang, B.; Clarke, D. Laboratory Investigation into Mechanical Properties of Cement Emulsified Asphalt Mortar. *Constr. Build. Mater.* **2014**, *65*, 76–83. [CrossRef]
11. Wang, H.; Wang, J.; Chen, J. Micromechanical Analysis of Asphalt Mixture Fracture with Adhesive and Cohesive Failure. *Eng. Fract. Mech.* **2014**, *132*, 104–119. [CrossRef]
12. Zhang, J.; Li, X.; Liu, G.; Pei, J. Effects of Material Characteristics on Asphalt and Filler Interaction Ability. *Int. J. Pavement Eng.* **2019**, *20*, 928–937. [CrossRef]
13. Zhang, X.; Chen, E.; Li, N.; Wang, L.; Si, C.; Wang, C. Micromechanical analysis of the rutting evolution of asphalt pavement under temperature–stress coupling based on the discrete element method. *Constr. Build. Mater.* **2022**, *325*, 126800. [CrossRef]
14. Tan, Y.; Guo, M. Using surface free energy method to study the cohesion and adhesion of asphalt mastic. *Constr. Build. Mater.* **2013**, *47*, 254–260. [CrossRef]
15. Yang, Q.; Xiao, S.L.; Qiu, X.; Luo, X.H.; Wang, Y.J. Mechanics Mechanism Analysis of Asphalt-Aggregate Interface Damage. *Key Eng. Mater.* **2015**, *667*, 359–364. [CrossRef]
16. Guo, F.; Pei, J.; Zhang, J.; Xue, B.; Sun, G.; Li, R. Study on the adhesion property between asphalt binder and aggregate: A state-of-the-art review. *Constr. Build. Mater.* **2020**, *256*, 119474. [CrossRef]
17. Kakar, M.R.; Hamzah, M.O.; Akhtar, M.N.; Woodward, D. Surface free energy and moisture susceptibility evaluation of asphalt binders modified with surfactant-based chemical additive. *J. Clean. Prod.* **2016**, *112*, 2342–2353. [CrossRef]
18. Ghabchi, R.; Singh, D.; Zaman, M. Evaluation of moisture susceptibility of asphalt mixes containing RAP and different types of aggregates and asphalt binders using the surface free energy method. *Constr. Build. Mater.* **2014**, *73*, 479–489. [CrossRef]
19. Vassaux, S.; Gaudefroy, V.; Boulangé, L.; Pévère, A.; Mouillet, V.; Barragan-Montero, V. Towards a better understanding of wetting regimes at the interface asphalt/aggregate during warm-mix process of asphalt mixtures. *Constr. Build. Mater.* **2017**, *133*, 182–195. [CrossRef]
20. Fang, Y.; Zhang, Z.; Zhang, H.; Li, W. Analysis of wetting behavior and its influencing factors of rejuvenator/old asphalt interface based on surface wetting theory. *Constr. Build. Mater.* **2022**, *314*, 125674. [CrossRef]
21. Qin, Z.Y.; Gao, Q.G.; Zhang, S.F.; Li, J.Z. Surface Free Energy and Dynamic Wettability of Differently Machined Poplar Woods. *BioResources* **2014**, *9*, 3088–3103. [CrossRef]
22. Wang, A.; Shen, S.; Li, X.; Song, B. Micro-surfacing mixtures with reclaimed asphalt pavement: Mix design and performance evaluation. *Constr. Build. Mater.* **2019**, *201*, 303–313. [CrossRef]
23. Zhu, J.; Ma, T.; Fan, J.; Fang, Z.; Chen, T.; Zhou, Y. Experimental study of high modulus asphalt mixture containing reclaimed asphalt pavement. *J. Clean. Prod.* **2020**, *263*, 121447. [CrossRef]

24. Liu, X.; Chen, S.; Ma, T.; Wu, X.; Yang, J. Investigation of Adhesion Property between Asphalt Binder and Aggregate Using Modified Boiling Methods for Hot and Wet Area. *J. Mater. Civ. Eng.* **2023**, *35*, 04022467. [CrossRef]
25. Adams, D.F.; Walrath, D.E. Further development of the losipescu shear test method. *Exp. Mech.* **1987**, *27*, 113–119. [CrossRef]
26. Zhou, L.; Huang, W.; Xiao, F.; Lv, Q. Shear adhesion evaluation of various modified asphalt binders by an innovative testing method. *Constr. Build. Mater.* **2018**, *183*, 253–263. [CrossRef]
27. Moraes, R.; Velasquez, R.; Bahia, H. Using bond strength and surface energy to estimate moisture resistance of asphalt-aggregate systems. *Constr. Build. Mater.* **2017**, *130*, 156–170. [CrossRef]
28. Huang, W.; Zhou, L. Evaluation of Adhesion Properties of Modified Asphalt Binders with Use of Binder Bond Strength Test. *Transp. Res. Rec. J. Transp. Res. Board* **2017**, *2632*, 88–98. [CrossRef]
29. Lv, Q.; Huang, W.; Xiao, F. Laboratory evaluation of self-healing properties of various modified asphalt. *Constr. Build. Mater.* **2017**, *136*, 192–201. [CrossRef]
30. Moraes, R.; Velasquez, R.; Bahia, H.U. Measuring the Effect of Moisture on Asphalt–Aggregate Bond with the Bitumen Bond Strength Test. *Transp. Res. Rec.* **2011**, *2209*, 70–81. [CrossRef]
31. Bionghi, R.; Shahraki, D.; Ameri, M.; Karimi, M.M. Correlation between bond strength and surface free energy parameters of asphalt binder-aggregate system. *Constr. Build. Mater.* **2021**, *303*, 124487. [CrossRef]
32. Yue, Z.Q.; Bekking, W.; Morin, I. Application of Digital Image Processing to Quantitative Study of Asphalt Concrete Microstructure. *Int. J. Pavement Res. Technol.* **2014**, *7*, 410–416.
33. Ye, F.; Yin, W.; Lu, H. A model for the quantitative relationship between temperature and microstructure of Styrene–Butadiene–Styrene modified asphalt. *Constr. Build. Mater.* **2015**, *79*, 397–401. [CrossRef]
34. Yin, W.; Ye, F.; Lu, H. Establishment and experimental verification of stability evaluation model for SBS modified asphalt: Based on quantitative analysis of microstructure. *Constr. Build. Mater.* **2017**, *131*, 291–302. [CrossRef]
35. Ye, F.; Yin, W.; Lu, H.; Dong, Y. Property improvement of Nano-Montmorillonite/SBS modified asphalt binder by naphthenic oil. *Constr. Build. Mater.* **2020**, *243*, 118200. [CrossRef]
36. Yuan, J.; Lu, H.; Yin, W.; Wu, Y. Influences of Naphthenic Oil on SBS-Modified Asphalt Binder. *J. Mater. Civ. Eng.* **2019**, *31*, 04019162. [CrossRef]
37. Xiao, R.; Polaczyk, P.; Wang, Y.; Ma, Y.; Lu, H.; Huang, B. Measuring moisture damage of hot-mix asphalt (HMA) by digital imaging-assisted modified boiling test (ASTM D3625): Recent advancements and further investigation. *Constr. Build. Mater.* **2022**, *350*, 128855. [CrossRef]
38. Alayat, A.B.; Ali Omar, H. Pavement Surface Distress Detection Using Digital Image Processing Techniques. *J. Kejuruter.* **2023**, *35*, 247–256. [CrossRef] [PubMed]
39. *ASTM D244*; Standard Test Methods and Practices for Emulsified Asphalts. ASTM International: West Conshohocken, PA, USA, 2023.
40. *ASTM D5*; Standard Test Method for Penetration of Bituminous Materials. ASTM International: West Conshohocken, PA, USA, 2020.
41. *ASTM D113*; Standard Test Method for Ductility of Asphalt Materials. ASTM International: West Conshohocken, PA, USA, 2023.
42. *ASTM D2170*; Standard Test Method for Kinematic Viscosity of Asphalts. ASTM International: West Conshohocken, PA, USA, 2022.
43. *ASTM D36*; Standard Test Method for Softening Point of Bitumen (Ring-and-Ball Apparatus). ASTM International: West Conshohocken, PA, USA, 2020.
44. Ding, D.; Gong, M.; Chen, J.; Sun, Y.; Tai, N. Factors influencing static and dynamic rheological properties of cement emulsified asphalt composite binder. *Constr. Build. Mater.* **2020**, *264*, 120257. [CrossRef]
45. Liu, Y.; Zhang, Z.; Tan, L.; Xu, Y.; Wang, C.; Liu, P.; Yu, H.; Oeser, M. Laboratory evaluation of emulsified asphalt reinforced with glass fiber treated with different methods. *J. Clean. Prod.* **2020**, *274*, 123116. [CrossRef]
46. Song, B.; Springer, J. Determination of Interfacial Tension from the Profile of a Pendant Drop Using Computer-Aided Image Processing: 2. Experimental. *J. Colloid Interface Sci.* **1996**, *184*, 77–91. [PubMed]
47. Song, B.; Springer, J. Determination of Interfacial Tension from the Profile of a Pendant Drop Using Computer-Aided Image Processing: 1. Theoretical. *J. Colloid Interface Sci.* **1996**, *184*, 64–76. [PubMed]